PROCEEDINGS, Twenty-Eight Workshop on Geothermal Reservoir Engineering
Stanford University, Stanford, California, January 27-29, 2003
SGP-TR-173

HYDRAULIC FRACTURE PROPAGATION NEAR A NATURAL DISCONTINUITY

V. Koshelev and A. Ghassemi

Department of Geology & Geological Engineering
University of North Dakota
Grand Forks, ND 58202

ABSTRACT

The trajectory of a hydraulically driven crack near natural fractures, faults, and inhomogeneities has been studied using the complex variable hypersingular boundary element technique. The crack trajectories are presented for the cases of an oblique and a steeply inclined fault. It has been demonstrated that natural fractures, faults, and other inhomogeneities generate unstable fracture configurations which can transform significantly under small disturbances of the initial crack inclination, loading, and geometry. The mutual influences of a propagating crack, a fault, and material inhomogeneity are also discussed.

INTRODUCTION

Hydraulic fracture growth in naturally fractured rock is an important issue for geothermal energy extraction. Particularly when dealing with enhanced geothermal systems. It is of great interest to know when a fracture begins to grow, what is the direction of crack propagation, and how will the propagating fracture interact with natural discontinuities? What would be the magnitude of shear slip on the natural fracture (if any) and how will the slip impact fracture permeability? And finally, will the fracture cross existing discontinuities or will it be terminated? Answers to these questions can assist in assessing the outcome of hydraulic fracture stimulation practices in geothermal reservoirs. In search for answers to these questions, one must deal with numerous factors making the problem rather complicated. Thus, we are developing a model capable of dealing with crack propagation near natural discontinuities such as joints and faults. The complex variable boundary element method (CV-BEM) has proven to be the more effective instrument in fracture studies mainly because it provides a higher accuracy and reduces the problem dimensionality by one (thus, for example, a 3D problem is solved in 2D). Whereas previous studies (Linkov and Mogilevskaya, 1998; Mogilevskaya, 1997) require introduction of a modified incremental procedure for choosing the direction of crack growth; we exploit the method developed by Dobroskok (2001).

Fracture Propagation Scheme

Consider a crack emanating from a wellbore in the vicinity of a fault (Figure 1). The radius of the wellbore is R; the crack has an initial length ℓ and makes an angle of α with the y-axis. The distance from the center of the wellbore to the fault is d, the angle of the fault with the y-axis is ϕ, and the fault has a length of $20R$. When considering a crack without the wellbore, the fault length is ten times the length of the initial crack.

It is further assumed that the initial crack is small enough not to propagate if it and the wellbore are not internally pressurized ($p = 0$). Then, the pressure p increases from zero up to the value sufficient for crack propagation in mode I in accordance with the criterion $K_I = K_{IC}$. The problem is reduced to finding the crack trajectory, displacement discontinuities, and the tractions on the fault surface given that (i) σ_H and σ_h are prescribed at infinity, (ii) fracture propagation is governed by the condition $K_I = K_{IC}$, and (iii) the condition on the fault is specified.

We described the fault by Coulomb's law with cohesion c and a friction angle ρ. If the normal traction on some part of the fault becomes tensile due to the influence of the approaching crack, the tractions are set to zero on that part to reflect its opening. When searching for the crack trajectory in the close vicinity of a fault, a more general concept of interaction between the fault surfaces should be considered to include fault cohesion and its deterioration under loading. In this way, the stress is redistributed due to the approaching fracture and the growing load so that the

fault gradually is transferred into a sliding state. However, to evaluate the role of friction, we consider examples using the cohesionless Coulomb's relation:

$$\sigma_{nt} = f \cdot \sigma_{nn} \frac{\Delta u_t}{\mid \Delta u_t \mid} \qquad (1)$$

where σ_{nt} and σ_{nn} are tangential and normal tractions on the fault surface, Δu_t is the tangential displacement discontinuity; $f = \tan \rho$, where ρ is the friction angle. This condition refers to the limiting case when the whole fault is in the plastic state.

Using the CVH-BEM algorithm described in Dobroskok (2001), we automatically calculate both the crack path and changes on the fault surfaces. In most of the examples we consider the fracture faces is loaded by a fluid pressure (this is the case of slow pressurization). For the fast pressurization case we assume closed fracture surfaces (practically, this means that $|\Delta u_n| \ll |\Delta u_t|$) only the tip element is open, and the fracture faces are frictionless: $|\sigma_{nt}| \ll |\sigma_{nn}|$. We suppose that the length of the preexisting fault or joint and its inclination are known in advance. For a natural fault we use the same type of boundary conditions as for a rapidly pressurized cracks.

APPLICATIONS

We first consider the trajectory of an isolated crack and investigate the dependence of the fracture trajectory on the angle α measuring the inclination of the preexisting crack relative to the vertical axis or the direction of the maximum principal stress at infinity. Then, we will study its behavior near a fault (Figure 1). For the isolated crack problem we consider the crack half-length to be $\ell = 0.16$ m and assume that $K_{IC} = 2$ MPa$\sqrt{\text{m}}$, and $\sigma_H = 12$ MPa, $\sigma_h = 10$ MPa. When considering the wellbore/crack problem we assume that $\frac{\ell}{R} = 0.1$ and define a dimensionless parameter $\beta = \frac{(\sigma_H - \sigma_h)\sqrt{R}}{K_{IC}}$ controlling the fracture path (Mogilevskaya et al., 2000). In both problems, the fluid pressure is allowed to increase until the critical condition $K_I = K_{IC}$, thereafter it is kept constant during the fracture propagation.

It can be seen in Figure 2 that as expected, the isolated crack turns in the direction of maximum in-situ stress. This example dealt with the simplest case of an unstable crack configuration and the results could be expected by taking into account the symmetry of the geometry and the loading conditions.

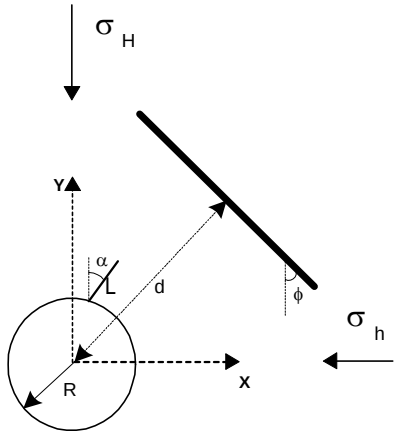

Figure 1: Problem geometry for fracture propagation from a wellbore in the vicinity of a fault.

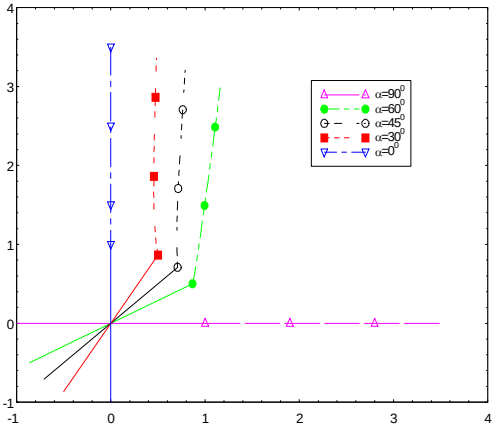

Figure 2: The trajectories of and isolated cracks under fluid pressure (slow rate of loading.

Interaction of a Crack and a Fault

Fracture propagation near a natural discontinuity is an important problem in modeling

hydraulic fracture propagation in a reservoir with natural fractures. However, the modeling approach in Linkov and Mogilevskaya (1998) cannot be used to treat this problem; we use a different numerical approach to address two non-linear effects namely, changes in geometry caused by the growing cracks and irreversible deformations on the fault surfaces. These effects are simultaneously accounted for by using a method discussed in Dobroskok (2001). This method has been implemented in CVBEM of Linkov and Mogilevskaya (1998) and is used herein.

Again, we defined $\beta = \frac{(\sigma_H - \sigma_h)\sqrt{d}}{K_{IC}}$ with $d = 1.5\ell\sqrt{2}$, consider σ_H and σ_h to be constant, and increase the fluid pressure up to a critical value to satisfy the condition $K_I = K_{IC}$. For the examples of this section we let $K_{IC} = 2\text{MPa}\cdot\sqrt{\text{m}}$, $\sigma_H = 12$ MPa, $\sigma_h = 10$ MPa, and consider frictionless sliding of the fault. The initial fracture half-length is assumed to be $\ell = 0.56$ m and $\ell = 0.06$ m in the different cases that follow.

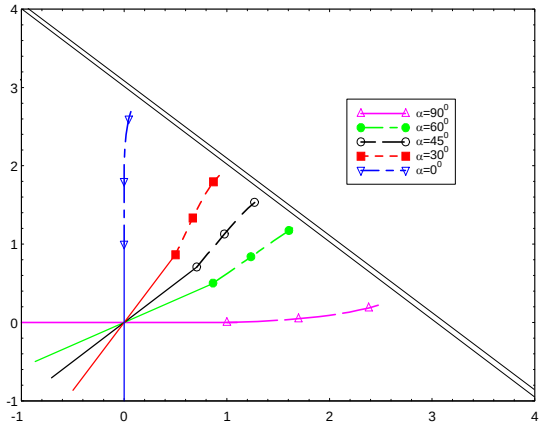

Figure 3: Fractures trajectories in close vicinity of a fault ($\beta = 1.19$).

Figures 3-7 illustrate the simulation results for a crack propagating in the vicinity of a fault. It is evident that the fault, as a surface with discontinuity of tangential displacement (slip) modifies the stress fields near the crack tip and the crack opening. Therefore, we observe deflections of the fractures trajectories from the direction of maximum far-field stress when they approach the fault. Figure 3 corre-

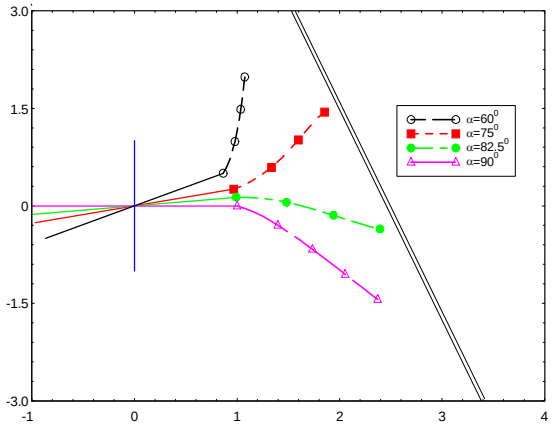

Figure 4: Fractures trajectories in the close vicinity of a steeper fault ($\ell = 0.56$ m).

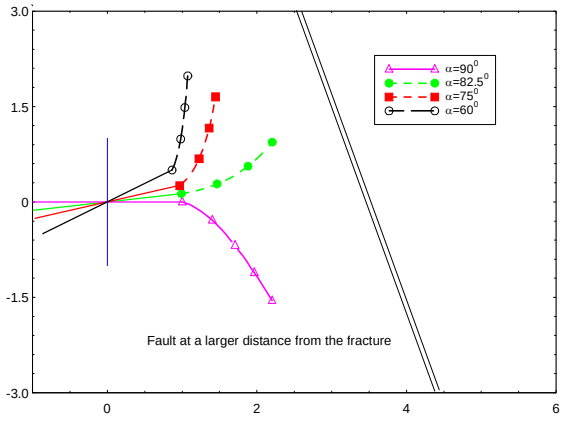

Figure 5: The role of initial crack length ($\ell = 0.06$ m).

sponds to a fault that is inclined to the y-axis by an angle $\varphi = 45^0$. We see that the fracture trajectories change considerably due to the presence of the fault. There is no tendency for them to turn towards the y-axis (compare with Figure 2). The next example (Figure 4) illustrates the role of the steepness of the fault. Now $\varphi = 18^0$, and the shear stresses induced by the fault become more important. For some initial cracks, the possibility of intersecting the fault is reduced. One can observe that there is an angle α_* ($75^0 < \alpha_* < 90^0$) which determines the unstable crack configuration; for $\alpha = \alpha_*$, small disturbances of the parameters lead to a sharp deflection of the propagation trajectory.

Figure 5 demonstrates the influence of the preexisting crack length. We have the same angle $\varphi = 18^0$ as in the previous case. Decreasing the crack length and increasing the distance to the fault accentuates the impact of the in-situ stress contrast, however, there are no essential changes in the cracks' behavior.

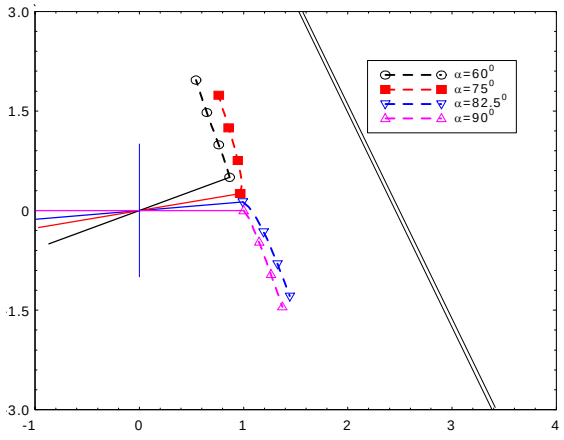

Figure 6: Trajectories for a modified stress contrast $\sigma_H - \sigma_h = 6$ MPa, $\ell = 0.56$ m (compare with Figure 4).

The next two series of graphs (Figures 6-7) depict the trajectories corresponding the case of $(\sigma_H - \sigma_h) = 6$ MPa. The other parameters are equal to those of the previous cases (Figure 4 and Figure 5). As expected, the essential difference consists only in sharper turning of the trajectories when $(\sigma_H - \sigma_h)$ is larger. It

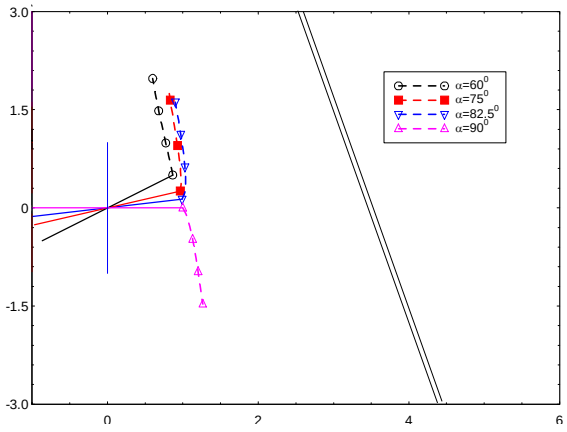

Figure 7: Trajectories near a steeper fault with $\sigma_H - \sigma_h = 6$ MPa, $\ell = 0.06$ m (compare with Figure 5).

should be noted that if we change the direction of σ_H and σ_h, in the case of φ =45^0, the complete scheme, and as a result the trajectories, rotate by an angle of 90^0. For the case of φ=18 one can expect that the cracks will more readily follow the far-field stress direction.

The Influence of Friction Figures 8-9 depict the results of modeling the trajectories near a frictional fault whose surfaces experience sliding. The friction parameter f is equal to 0.5 and 2, respectively. The geometric features of the propagation scheme are the same as that in Figure 4. We see that the friction leads to the rotation of the trajectories towards the $x-$axis promoting intersection with the fault. Also, the critical inclination angle of the preexisting crack is more than that in the frictionless case; $82.5^0 < \alpha_* < 90^0$ for $f = 0.5$.

It should be mentioned that the effects of sliding strongly depend on the angle φ and the ratio $\frac{\sigma_H}{\sigma_h}$. The elementary static analysis leads to this conclusion. In the case of symmetry when $\varphi = 0^0$ or 90^0 and the fracture propagates normal to the fault, there is no sliding at all.

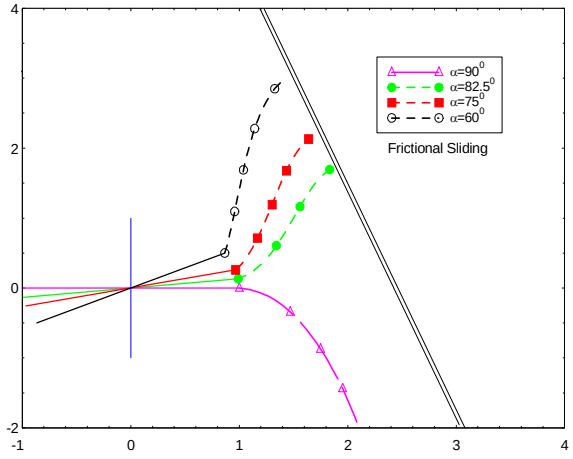

Figure 8: The effect of friction (small friction angle).

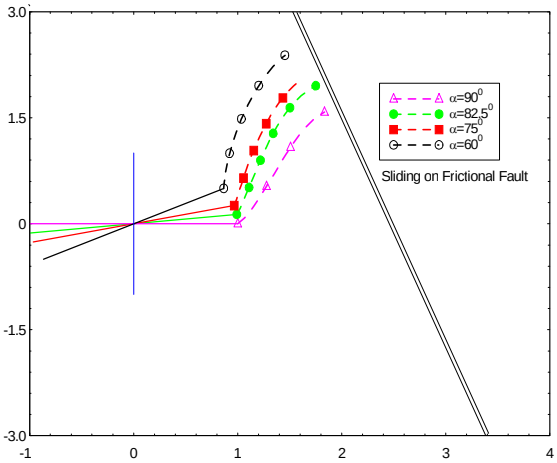

Figure 9: The effect of friction (larger friction angle).

Crack Emanating from a Wellbore

Now we modify the schemes of the previous section and consider the wellbore explicitly in the crack and fault interaction problem (Figure 1). Again, we vary the inclination of a preexisting crack relative to the vertical, α, and assume the wellbore radius is $R = 0.1$ m, $\ell = 0.01$ m, $K_{IC} = 0.5$ MPa$\cdot$m$^{\frac{1}{2}}$; and $\sigma_H = 22$ MPa, $\sigma_h = 11$ MPa. The fluid pressure is allowed to increase until the critical condition $K_I = K_{IC}$. Figures 10-11 illustrate the cracks trajectories near a fault under the same loading path as in Figure 3 and 4, respectively. As a result, new trajectories deviate more noticeably near the well and turn to become oriented parallel to the fault (the dashed lines illustrate the crack paths when no fault is present). Intersection with the fault is not promoted for initial cracks that are not sub-parallel to the $x-$direction. However, as shown in Figure 12, when the wellbore is rapidly pressurized the cracks tend to follow their initial direction and possibly intersect the fault.

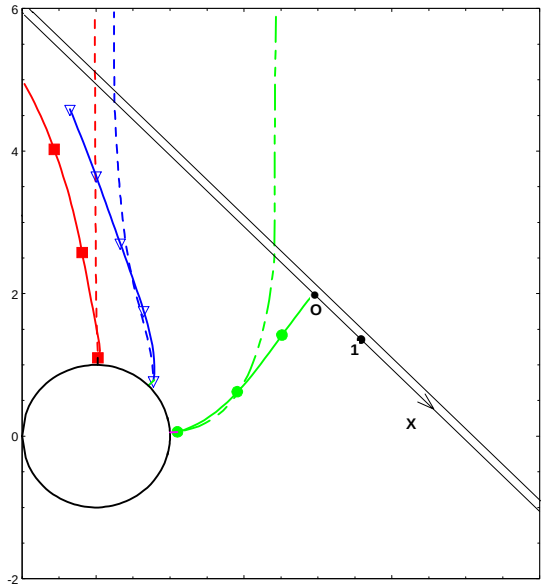

Figure 10: Crack propagation from wellbore near fault, ($\beta = 3.95$).

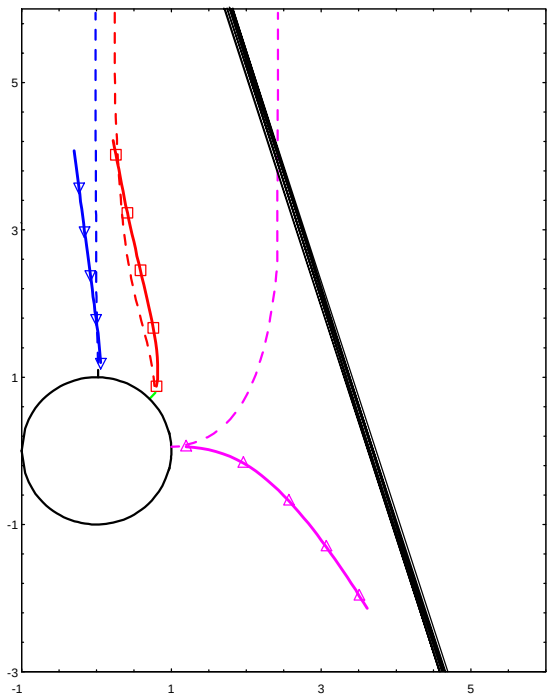

Figure 11: Crack emanating from a wellbore near a steep fault, $\beta = 3.95$.

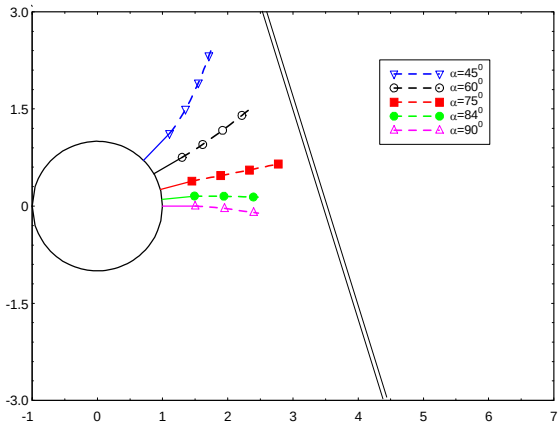

Figure 12: Fast pressurization rate, with $\sigma_H = 15$ MPa, $\sigma_H = 10$, MPa, $K_{IC} = 2$ MPa·m$^{\frac{1}{2}}$ ($\beta = 0.79$).

A Fracture Near Inhomogeneities

The general features of cracks trajectories near inclusions have been studied rather well (Mogilevskaya et al., 2000). We now study the combined influence of two factors: rigidity of a seam-like inhomogeneity and sliding effects at the interface. Figure 13 presents a scheme of the crack approaching the interface. We model an inhomogeneous structure by two rectangular blocks whose lengths are ten times the initial crack length (so that we exclude the effect of block size). As in the previous sections we consider the crack growth under internal loads (slow pressurization mode) and fixed the in-situ stresses. We suppose that the crack starts from the "lower" layer with the Young's modulus E_2 and Poisson's ratio ν_2 and approaches the "upper" layer characterized by E_1 and ν_1. The layers (blocks) are imbedded in an infinite elastic domain with E_0, ν_0.

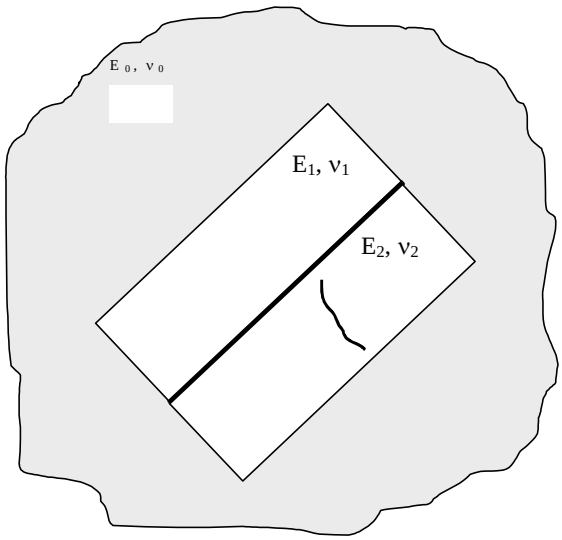

Figure 13: A hydraulic fracture approaching an interface between layers having different moduli.

Bellow we consider the combinations of two factors: (i) the relative rigidity of the blocks: rigid upper block, $\frac{E_1}{E_2} = 3$ and softer upper block, $\frac{E_2}{E_1} = 3$; (ii) the conditions on the contact between blocks: (a) full cohesion and (b) frictionless sliding. All examples refer to the case where $E_1 = E_0$ and $\nu_1 =$

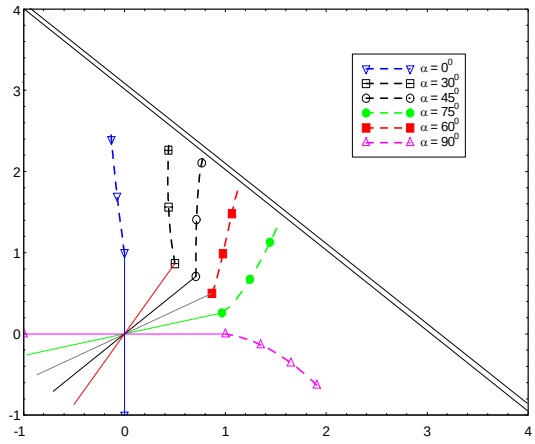

Figure 14: Fractures behavior near the soft layer; interface has perfect cohesion.

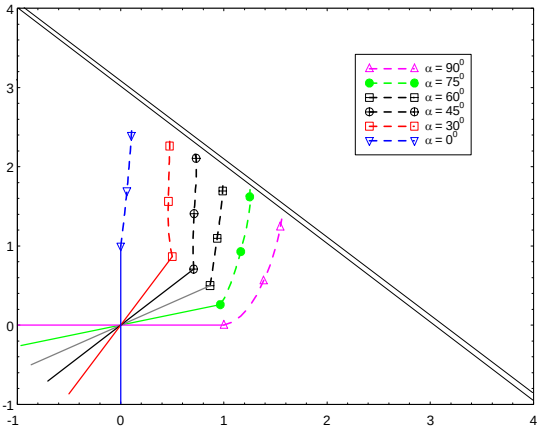

Figure 15: Fractures behavior near the rigid layer; interface has perfect cohesion.

$\nu_2 = \nu_0 = 0.3$. The present problem geometry is the same as on the Figure 3; with $\varphi = 45^0$; $d = 1.5\ell\sqrt{2}$. The coordinate axes coincides with the directions of the main in-situ stresses. We remind the reader that every figure presents a number of fracture paths differing by the inclination of the preexisting crack.

Figures 14-15 illustrate the role of rigidity of the layers with perfect cohesion at their interface. One can see that a softer "upper" layer leads to a repelling effect for some initial crack orientations (Figure 14). The case of the rigid "upper" layer (Figure 15) demonstrates behavior opposite to that of a soft one. Overall, the rigid layer appears to attract the cracks to the interface.

The sliding in the case of the soft upper block (Figure 16) leads to an amplification of the repelling. For the case of the rigid upper block (Figure 17) there is a slight attracting effect. However, in both cases repelling may be manifest in very close vicinity of the interface. This issue needs to be studies further.

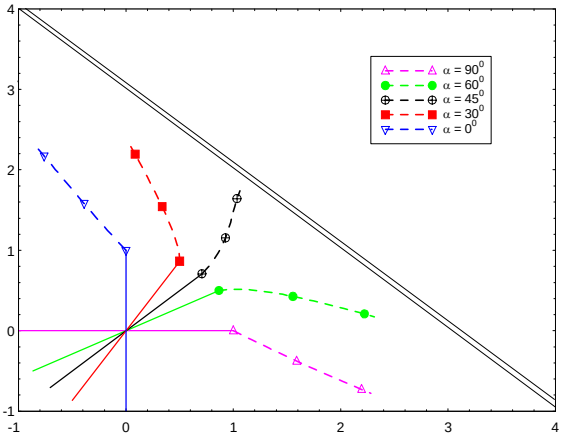

Figure 16: Effect of sliding of the softer layer.

SUMMARY AND CONCLUSIONS

The Complex Variable Hypersingular Boundary Element Method has been used for studying hydraulic fracturing near natural fractures, faults, and inhomogeneities. We have demonstrated that natural fractures, faults, and other inhomogeneities generate unstable fracture configurations which can transform significantly under small disturbances of the initial crack

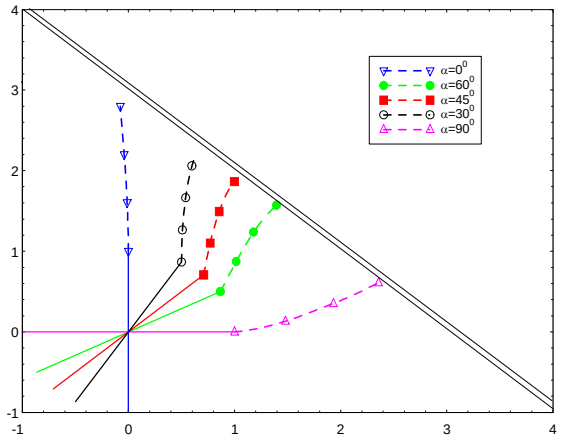

Figure 17: Effect of sliding of the more rigid layer.

inclination, loading, and geometry. The fault inclination and frictional characteristics as well the conditions on the fracture surfaces proved to be the most significant factors that influence the trajectories. A number of examples illustrate a variety of fracture behavior near a natural discontinuity such as a fault. Formulation and solution of the fracture arrest or "jog" at the interface should follow the analysis of the fracture trajectory once it is determined whether it is attracted or rejected by the interface. Future improvements should address a more general concept of interaction, i.e., consideration of the successive process of loss of cohesion on the fault surface as the fracture propagates towards it. Also, special asymptotics need to be implemented near the tip depending on the interface characteristics near the tip.

ACKNOWLEDGMENTS

The authors wish to gratefully acknowledge the financial support of the U.S. DOE (DE-FG07-99ID13855) and DOD (N-68936-02-C-0214).

REFERENCES

Dobroskok, A.A., 2001. On a new method for iterative calculation of crack trajectory. Int. J. Fracture, 111, 41-46.

Linkov A.M., Mogilevskaya S.G., 1998. Complex hypersingular BEM in plane elasticity problems. In: Sladek, V. and J. Sladek (eds), Singular Integrals in Boundary Element Methods. Computational Mechanics Publications, Southampton, 299-364.

Mogilevskaya S.G., Rothenburg L., Dusseault M.B., 2000. Growth of pressure-induced fractures in the vicinity of a wellbore. Int. J. Fracture, 104, 25-30.

Mogilevskaya S.G., 1997. Numerical modeling of 2-D smooth crack growth. Int. J. Fracture, 87, 389-405.